Supersaturation and crystallization behaviors of rare-earth based cuprate superconducting films grown by chemical solution deposition

Jiangtao Shi [a,b], Yue Zhao [a,c,*], Yue Wu [a], Manuela Erbe [b], Chunjiang Guo [a], Jingyuan Chu [d], Guangyu Jiang [c], Jens Hänisch [b], Bernhard Holzapfel [b], Zhijian Jin [a]

[a] School of Electronic Information and Electrical Engineering, Shanghai Jiao Tong University, 200240 Shanghai, People's Republic of China
[b] Institute for Technical Physics (ITEP), Karlsruhe Institute of Technology (KIT), Eggenstein-Leopoldshafen, Germany
[c] Shanghai Superconductor Technology Co., Ltd., 200240 Shanghai, People's Republic of China
[d] China Triumph International Engineering Co. Ltd., 200063 Shanghai, People's Republic of China

Keywords:
Supersaturation
Textured growth
Diffusion
Chemical solution deposition
YBCO

A B S T R A C T

Chemical solution deposition is widely used in the preparation of rare-earth-based cuprate superconducting thin films, namely $RE_xBa_2Cu_3O_{7-y}$ (*RE* rare earth element). The crystallographic orientation of the films is strongly dependent on the degree of supersaturation during crystallization. In this paper, we systematically studied the crucial factors affecting supersaturation, such as the type and stoichiometry of the rare earth element and the sintering temperature. Furthermore, the relationship between *c*-axis orientation and supersaturation was established. The results demonstrate that a small *RE* ionic radius (e.g., *RE* Yb) and reduced *rE*-stoichiometry, studied on the example of yttrium, are beneficial for the growth of *c*-axis-oriented films at lower temperatures. In addition, a Y-O/Ba-Cu-O stacked-layer structure was proposed to regulate the diffusion distance to the reaction site. Compared with a Y-Ba-Cu-O single-layer, a *c*-axis orientation percentage of more than 40 % is achieved in the Y-O/Ba-Cu-O stacked-layer at even lower sintering temperatures. The results suggest that a low supersaturation is favorable to promote the growth of *c*-axis-oriented nuclei and therefore suppresses the growth of random orientations. This paper provides a new strategy to realize orientation modulation of rare-earth-based cuprate superconducting thin films by controlled chemical solution method.

1. Introduction

Chemical solution deposition (CSD) has been extensively studied in the field of functional thin films for many years [1–4]. A common feature of the CSD process is that the deposited film transforms from an amorphous intermediate/precursor to the desired crystalline state. It is well understood that the driving force of the transformation process depends on the supersaturation, which is closely related to the complex physical and chemical changes that occur during nucleation and film growth [5–7]. Therefore, fine-modulation of the supersaturation allows a better understanding of the amorphous-crystalline transformation in the CSD process.

With better mechanical [8,9] and magnetic [10–12] properties, rare-earth-based cuprate $RE_xBa_2Cu_3O_{7-y}$ (, *RE* = rare earth) superconducting tapes have been widely used [13–17]. Control of supersaturation has been successfully realized in the CSD route for the preparation of *RE*BCO superconducting films [18–20]. As previous studies demonstrated, the reaction path of the YBCO transformation varies with the solution chemistry. For example, in the trifluoroacetate-based metal–organic decomposition route (TFA-MOD), where the precursor solution and intermediary species in the film contain fluorine, the supersaturation is influenced by several key factors, such as the partial pressure of HF and H_2O, p_{HF} and p_{H2O}, the temperature, additives, etc. [21–28]. In the preparation of YBCO films by CSD, lower supersaturation was found to be favorable for *c*-axis nucleation [23,24], while the opposite was found for liquid phase epitaxy [29–31].

Due to increased environmental awareness, the use of fluorine has been questioned to some extent. Moreover, the slow growth rate (less than 10 nm/s) [32] of the TFA-MOD process is a pressing issue. An alternative, fluorine-free (FF) MOD process is attracting more and more attention in the field [33–36]. Compared to the conventional TFA-MOD method, the FF-MOD approach could be considered a "green" process, which even allows much higher growth rates up to 100 nm/s [37].

So far, the mechanisms of nucleation and growth of *RE*BCO

superconducting films by FF-MOD is not fully understood, though. A liquid phase of Ba-Cu-O is believed to form initially, followed by Y_2O_3 dissolving into the liquid phase [35,37]. Eventually, the *RE*BCO phase crystallizes with a preferred orientation on the substrate. Due to the completely different chemical reaction path, it is still unclear how to control supersaturation in the FF-MOD route. Therefore, a systematic study on the effect of supersaturation on nucleation and growth of *RE*BCO is very important, also for further understanding and optimization of the whole process.

In our previous studies, we synthesized stable, fluorine-free precursor solutions with different rare earth elements (*RE* = Yb, Y, Dy, Gd, Eu, and Sm) and good superconducting performance of the resulting *RE*BCO films [38]. In this paper, the first motivation is to understand how the degree of supersaturation affects the orientation of *RE*BCO deposited on CeO_2-buffered substrates. Moreover, we propose a multi-layer architecture of Ba-Cu-O and Y-O as a new strategy to regulate the distance of yttrium diffusion to the growth front. The *a*- and *c*-axis nuclei in the films were characterized by X-ray diffraction (XRD), Raman spectroscopy, and transmission electron microscopy (TEM). The diffusion behavior of yttrium in the liquid phase was investigated by TEM and time-of-flight secondary ion mass spectrometry (TOF-SIMS).

2. Experimental

2.1. Precursor synthesis

The precursor solutions of *RE*BCO, Ba-Cu-O and Y-O were synthesized using a fluorine-free propionate-based route, the details of which were reported in Refs [39,40]. For the Ba-Cu-O precursor, Ba- and Cu-acetates were dissolved in propionic acid in the ratio Ba:Cu = 2:3 with a total cation concentration of 0.2 mol/L, and for the Y-O precursor, Y-acetate is dissolved also in propionic acid with a cation concentration of 0.1 mol/L.

2.2. Film preparation

The films were deposited using a typical CSD process consisting of three main steps, namely dip coating, low-temperature pyrolysis, and high-temperature crystallization [38]. Flexible textured templates with an architecture of CeO_2/$LaMnO_3$/IBAD-MgO/Y_2O_3/Al_2O_3/C276 (provided by Shanghai Superconductor Technology) were used as substrate [41]. The respective precursor solutions were deposited on the substrate by dip-coating at a withdrawal speed of 1000 μm/s. Whereas the *RE*BCO precursor layer was deposited in the typical coating and pyrolysis procedure [38,42], for the composite film with the Y-O/Ba-Cu-O stacked-layer, dip-coating and pyrolysis were repeated several times to obtain the desired multilayer structure: First, Ba-Cu-O precursor solution was deposited, followed by a pyrolysis process at 500 °C, which was repeated five times to increase the Ba-Cu-O layer thickness. Then, the Y-O precursor solution was deposited on the pyrolyzed Ba-Cu-O layer followed by a similar coating and pyrolysis procedure. Eventually, the architecture of the composite film consists of 2 × (Y-O)/5 × (Ba-Cu-O). For comparison, both the Y-Ba-Cu-O single layer and the Y-O/Ba-Cu-O stacked layer were sintered at high temperatures in the range 740–860 °C with an oxygen partial pressure pO_2 of 50 ppm at 1 bar total pressure.

2.3. Structural characterization

Phase composition and crystallographic orientation of the films were characterized by a four-circle X-ray diffractometer equipped with a two-dimensional detector (Bruker D8 Advance, Cu-Kα radiation, λ = 1.5406 Å). The texture was also characterized by Raman spectroscopy (Renishaw inVia Qontor, Nd-YAG laser, λ = 532 nm). The TEM cross-sectional sample was prepared by conventional mechanical polishing and grinding, followed by ion milling. The TEM imaging and energy dispersive X-ray spectroscopy (EDXS) were performed using an aberration-corrected scanning transmission electron microscope (STEM, FEI Talos F200 X) with a double-tilt holder and a cold field emission source operated at 200 kV. A time-of-flight secondary ion mass spectrometer (TOF-SIMS, GAIA3) was operated under a 5 kV focused ion beam (FIB), and a 50 pA detector was used to measure the distribution of Y and Ba along the thickness of the film. Depth distribution information is obtained by combining TOF-SIMS measurements with FIB (milling/sputtering) to characterize a thin film structure. TOF-SIMS Explorer was used for the acquisition and analysis of the secondary ion signals. The data were acquired from 10 × 10 μm^2 scan areas in the positive ion detection mode. In order to avoid crater edge artifacts, the data analysis regions of interest were limited to the central 5 × 5 μm^2 areas.

Table 1
The *RE* ionic radii and peritectic temperatures of *RE*BCO for BaO:CuO of 3:5 [43].

RE element	Yb	Y	Dy	Gd	Eu	Sm
ionic radius (Å)	0.985	1.019	1.027	1.053	1.066	1.079
peritectic temperature (°C)	900	1000	1010	1030	1050	1060

3. Results and discussion

3.1. Rare-earth species, supersaturation and orientation

In contrast to the conventional TFA-MOD method, a transient Ba-Cu-O liquid phase is supposed to be present during the FF-MOD route. It plays an essential role for the YBCO phase evolution: it accelerates the crystallization and therefore enables an enhanced growth rate of the films. Our previous studies found that Y_2O_3 nano-particles form in the intermediate state after decomposition [35]. Y_2O_3 is very stable and has a high melting point. During high-temperature crystallization, Y_2O_3 tends to migrate toward the surface layer of the film. As the reaction proceeds, however, yttrium re-diffuses into the Ba-Cu-O liquid phase, according to reaction scheme 1, and consequently YBCO is formed by epitaxial nucleation and growth at the interface.

$$Y_2O_3\,(s) + \text{liquid}\,(Ba \quad Cu \quad O) \rightarrow YBa_2Cu_3O_{7-\delta}\,(s) + O_2(g)\uparrow \qquad (1)$$

In this diffusion-controlled process, reaction parameters such as the diffusion distance to the reaction site, *D*, and the concentration, *C*, of yttrium in the Ba-Cu-O liquid phase determine the supersaturation, *δ*, at the nucleation site, which is most likely close to the film-substrate interface. *δ* is the main driving force for the formation of YBCO. However, due to the fast growth rate and limited diffusion time, a certain enrichment of yttrium is still present in the upper layers of the YBCO film even after the reaction is complete [35]. Since yttrium segregation and re-dissolution are the forward and reverse directions of an equilibrium reaction, they occur simultaneously; their respective reaction rates, though, depend on the reaction conditions. For *RE*BCO films with different rare earth elements, the chemical reaction paths governed by this segregation/re-diffusion process are very similar in principle. However, type and stoichiometry of *RE* and the sintering temperature affect *δ* during the *RE*BCO phase formation and ultimately have a strong influence on the crystalline orientation.

For *RE*BCO bulk materials, the peritectic temperature of *RE*BCO was found to increase with the ionic radius of *RE*, as shown in Table 1 for a ratio BaO:CuO of 3:5 [43]. For thin films, the growth mode may be different, but the results on bulk samples may serve as guideline to understand the relationship between the *RE* element and supersaturation. For this study, we selected six rare earth elements (Yb, Y, Dy, Gd, Eu, and Sm), with small to large ionic radii of *RE*.

To shed light on the effect of rare earth type and stoichiometry on *δ*, a series of *RE*BCO films were was prepared by the FF-MOD method. We analyzed the degree of *c*-axis orientation in fully reacted *RE*BCO films

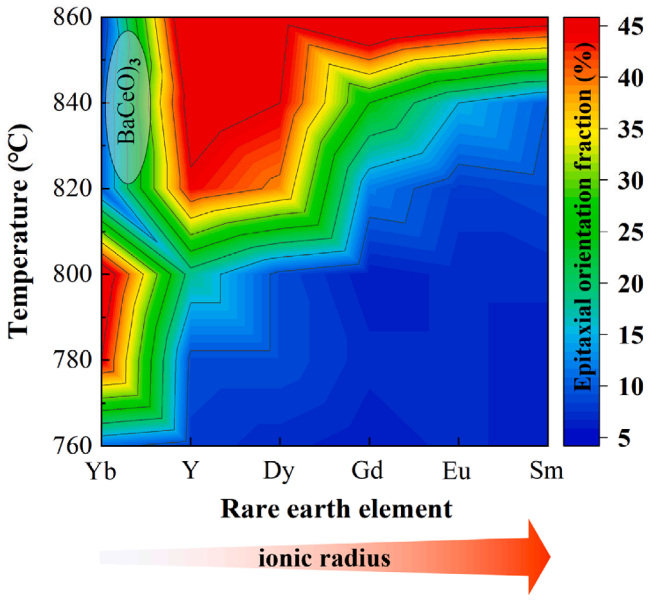

Fig. 1. Contour plot of the influence of *RE* ionic size and sintering temperature on f_X (Eq. (3)).

based on 2D XRD frames. According to our previous research, there are three texture components {006}, {103} and {200} in YBCO films, which we took into consideration for the evaluation, cf. Fig. 3. Moreover, the *c*-axis orientation represents the biaxial texture component [35,44]. According to literature reports [20], the epitaxy fraction is calculated by integrating the results of (005) *RE*BCO reflection at $\chi = 0^\circ$ (I_{epi}^{exp}) and $\chi \neq 0^\circ$ (I_{ring}^{exp}) in two-dimensional (2D) XRD 2θ – χ scans:

$$\frac{I_{random}}{I_{epitaxial}} = \frac{I_{ring}^{exp} \bullet (360/\Delta\chi) \bullet 4\pi}{8 \bullet I_{epi}^{exp}} \tag{2}$$

Therefore, we simply evaluated the trend coefficient of epitaxy orientation, f_X, using the integration results of (103) *RE*BCO reflection at $\chi \neq 0^\circ$ (I_{103}) and (006) REBCO reflection at $\chi = 0^\circ$ (I_{006}) in two-dimensional (2D) XRD 2θ χ scans:

$$f_X = \frac{I_{epitaxial}}{I_{epitaxial} + I_{random}} = \frac{8 \bullet I_{006}}{8 \bullet I_{006} + I_{103} \bullet (360/\Delta\chi) \bullet 4\pi} \tag{3}$$

The f_X values of various *RE*BCO films as a function of the sintering temperature and ionic radius of *RE*, Fig. 1, reveal that both parameters have a significant influence on the formation of *c*-axis-oriented *RE*BCO. In YbBCO films with a small *RE* ionic radius, f_X reaches values higher than 40 % at medium sintering temperatures between 770 °C and 810 °C. These are the lowest temperatures among all *RE*BCO films investigated in this study. Considerably higher sintering temperatures above 850 °C are required to obtain similarly high f_X values in SmBCO films. This comparison indicates that *c*-axis textured growth tends to decrease with increasing rare earth ion radius at a certain temperature. Furthermore, in the high temperature region (i.e., above 820 °C), the appearance of $BaCeO_3$ is clearly evident from the XRD results, indicating serious interfacial reactions. As a result, a part of the well-oriented *RE*BCO is consumed, seemingly reducing the f_X values.

According to the chemical reaction scheme 1 for the FF-MOD method, the relative proportion of *RE* in the Ba-Cu-O liquid phase should also have an effect on δ and thus on the preferential orientation of the films. Therefore, we investigated the relationship between *rE*-stoichiometry, *x*, the sintering temperature and the *c*-axis fraction, f_X, in $RE_xBa_2Cu_3O_{7-y}$ films on the example of YBCO in order to establish a correlation between *x* and δ. The ratio of Ba:Cu was fixed to 2:3, while the Y content *x* in $Y_xBa_2Cu_3O_{7-y}$ was varied, with $x = 0.8$, 1.0, 1.2 and 1.4. Fig. 2a shows the color-coded f_X values obtained for the four different levels of *x* in YBCO films sintered between 760 °C and 860 °C. At a temperature of 790 °C, the f_X value of the yttrium-poor film is already about 30 %. Larger concentrations of yttrium in the film require increasing temperatures for similarly high degrees of the preferential *c*-axis orientation. According to Fig. 2b [45], δ increases as the proportion of yttrium increases. Combined with our results, lower degrees of δ are therefore beneficial for the growth of *c*-axis oriented films.

A closer look at the raw data underlying Fig. 2 (a) shows that at low yttrium concentration and therefore low δ, a strong YBCO (006) peak appears, Fig. 3b, while the YBCO (103) peak is almost negligible, Fig. 3c. This indicates that low δ is favorable to promote the growth of *c*-axis orientated nuclei and suppress the growth of random orientation. With increasing yttrium content and δ, the intensity of the YBCO (006) peak decreases, Fig. 3e, while the intensity of the YBCO (103) peak increases, Fig. 3f. This means that random alignment has a competitive advantage over *c*-axis-oriented nuclei with increasing δ. At even higher levels of *x* and δ, the YBCO (006) peak, Fig. 3h, does not weaken any further, but the YBCO (200) peak, which represents *a*-axis-oriented grains, appears in addition to YBCO (103), Fig. 3h and i. This implies that *RE*BCO films with a specific crystallographic orientation can be obtained by modulating δ.

3.2. Effect of diffusion distance to the reaction site

The yttrium concentration in the Ba-Cu-O liquid phase obviously plays an important role for the orientation of the growing YBCO film, Figs. 2a and 3. During phase evolution in the FF-MOD route, yttrium segregates from the matrix as Y_2O_3 prior to the actual YBCO formation, but also re-dissolves when the yttrium concentration or solubility

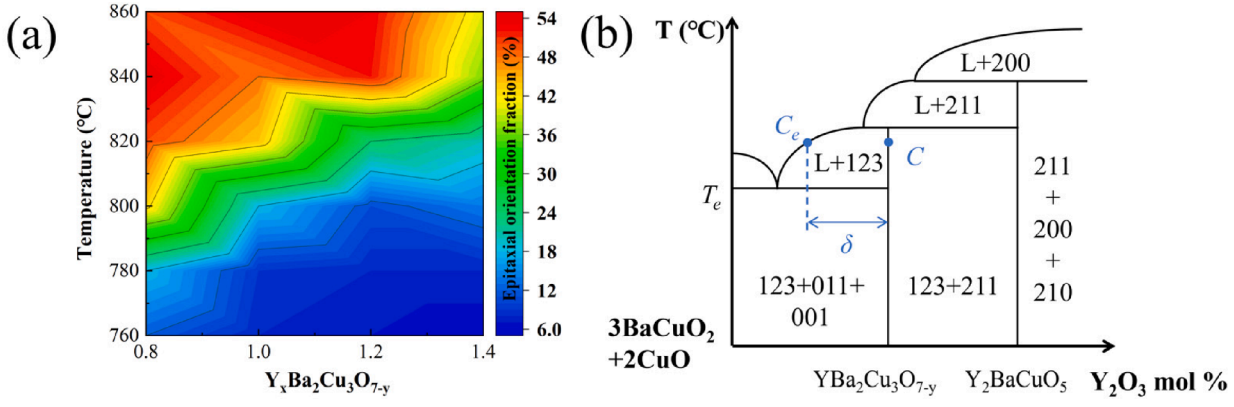

Fig. 2. (a) Contour plot of the influence of Y stoichiometry and sintering temperature on the f_X (color-coded in the bar to the right), (b) temperature phase diagram [45] of $BaCuO_2$-Y_2O_3. The phases in coexistence regions are labeled as follows: 200-Y_2O_3, 001-CuO, 011-$BaCuO_2$, 211-Y_2BaCuO_5, 123-$YBa_2Cu_3O_x$, 210-Y_2BaO_4.

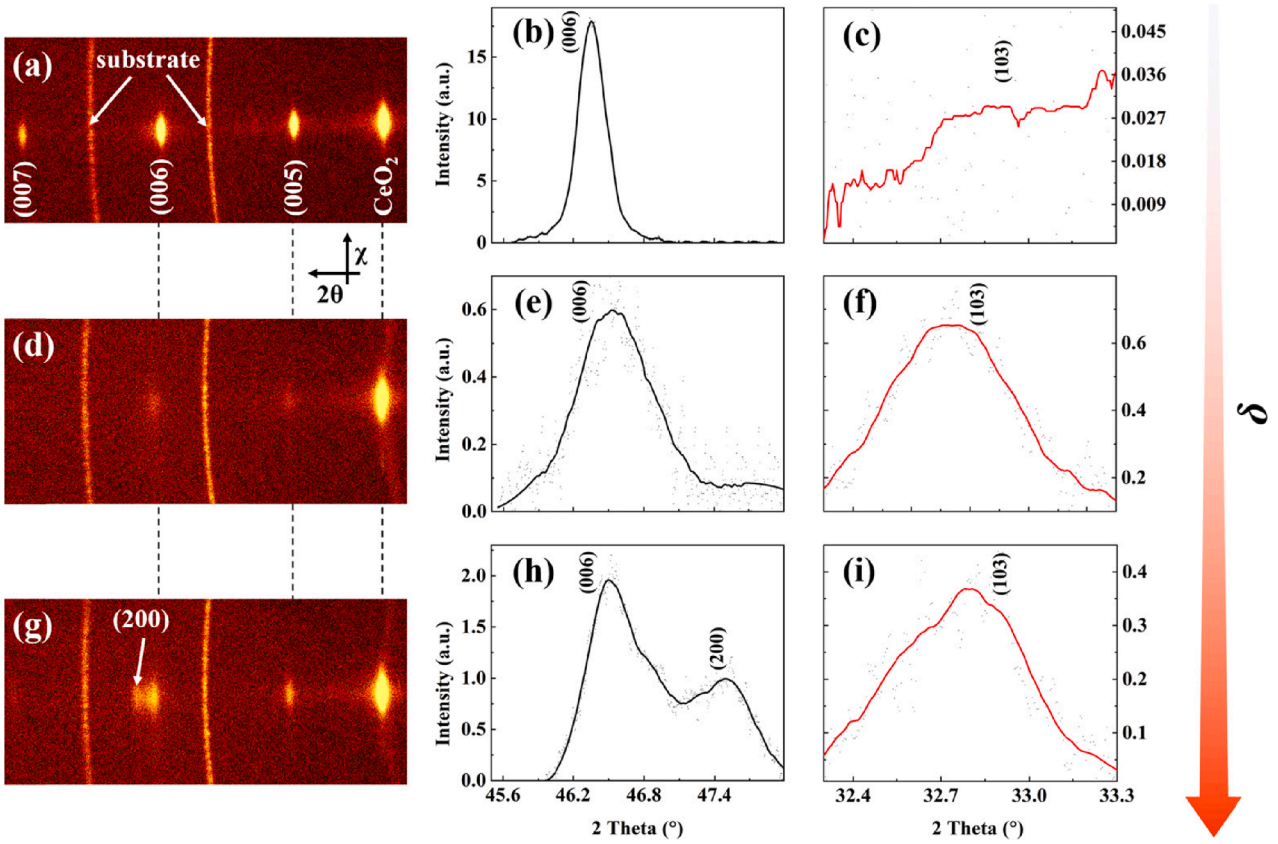

Fig. 3. XRD analysis of the effect of δ on the orientation of $Y_{0.8}Ba_2Cu_3O_{7-y}$, $Y_1Ba_2Cu_3O_{7-y}$ and $Y_{1.2}Ba_2Cu_3O_{7-y}$ films, respectively. (a) 2D GADDS X-ray diffraction patterns of $Y_{0.8}Ba_2Cu_3O_{7-y}$ film, (b) and (c) Integrated spectra from the XRD pattern of (a); (d) 2D GADDS X-ray diffraction patterns of $Y_1Ba_2Cu_3O_{7-y}$ film, (e) and (f) Integrated spectra from the XRD pattern of (d); (g) 2D GADDS X-ray diffraction patterns of $Y_{1.2}Ba_2Cu_3O_{7-y}$ film, (h) and (i) Integrated spectra from the XRD pattern of (g), where the arrow points in the direction of increasing δ.

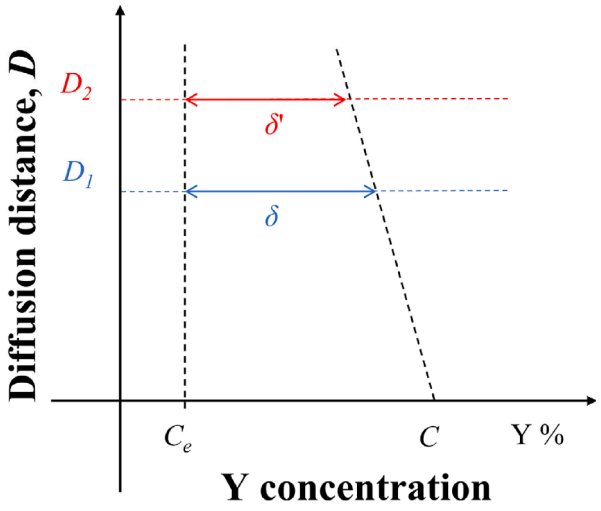

Fig. 4. Schematic diagram of the effect of different concentrations on the D of yttrium at the reaction interface, where C_e, C and δ represent the equilibrium concentration, the concentration of yttrium at the reaction interface and the supersaturation, respectively.

changes; the former affected e.g., by the beginning YBCO formation, the latter depends on external conditions such as temperature. Under specific conditions, however, the equilibrium concentration, i.e., the maximum possible concentration of yttrium, C_e, in Ba-Cu-O is a constant. Therefore, δ at the reaction site depends immediately on C. Besides, D also depends on C, Fig. 4, which shows a connection between D and δ. When the D increases from D_1 to D_2, δ decreases to δ', which means that larger D values can be considered equivalent to a lower yttrium concentration. Therefore, regulation of D offers another possibility for the modulation of δ. In our experiment, we increased D artificially by a special Y-O/Ba-Cu-O stacked-layer architecture, Fig. 5b, which we compared to a standard Y-Ba-Cu-O single-layer, Fig. 5a. Both types of samples were prepared via the same pyrolysis process. D is much smaller in the Y-Ba-Cu-O single-layer than in the Y-O/Ba-Cu-O stacked-layer architecture.

To investigate the effect of D, a comparative study was carried out on the two sets of films schematically depicted in Fig. 5a and b. In the Y-Ba-Cu-O single-layer, Y_2O_3 nanoparticles are mixed with other intermediate phases just after pyrolysis. During crystallization, the D of yttrium to the reaction site is extremely small within the Ba-Cu-O liquid phase in this case, practically negligible. In the early stage of the high-temperature process, nucleation at the interface is dominant, i.e., the Gibbs free energy at the interface is low compared to that in the film body. Y_2O_3 close to the interface dissolves into Ba-Cu-O, and YBCO starts crystallizing. In contrast, in the case of the Y-O/Ba-Cu-O stacked-layer, the yttrium source is far away from the interface. Hence, yttrium must diffuse through the entire Ba-Cu-O layer before nucleation can begin at the interface. Compared to the Y-Ba-Cu-O single-layer, the Y-O/Ba-Cu-O stacked-layer precursor therefore allows to play with the D of yttrium by adjusting the thickness of the Ba-Cu-O layer. It provides a new angle to study the effect of the D on the orientation of YBCO superconducting films.

To further investigate the effect of δ on the c-axis orientation of YBCO, XRD and Raman spectroscopy, were used to characterize the orientation quality of the sintered films. Raman spectroscopy makes it easy to analyze the homogeneity of the films by determining the

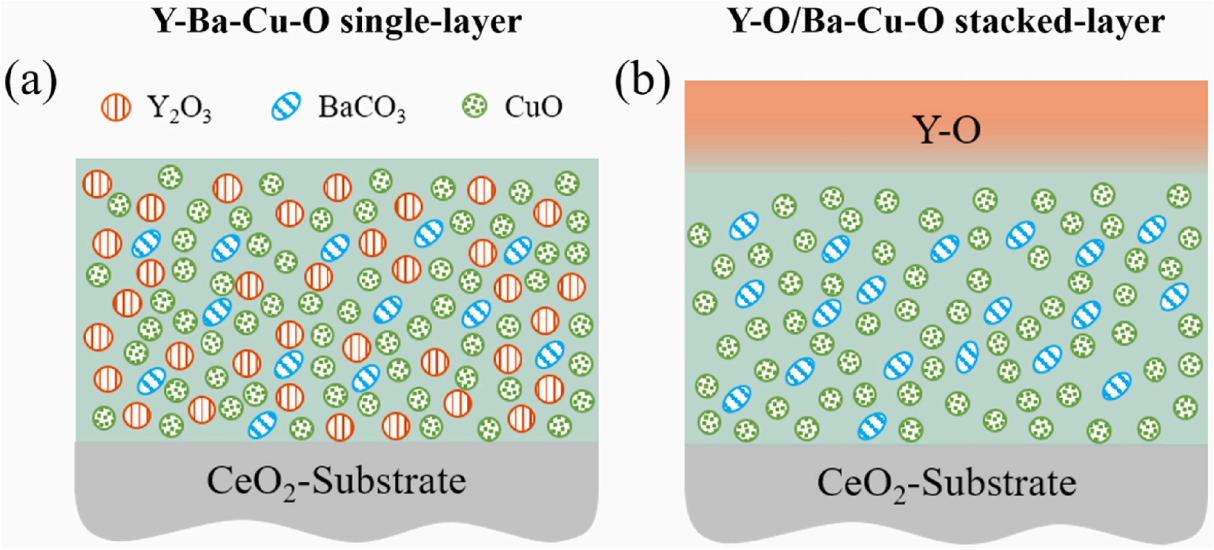

Fig. 5. Sketch of the architectures of (a) the Y-Ba-Cu-O single-layer and (b) Y-O/Ba-Cu-O stacked-layer after pyrolysis.

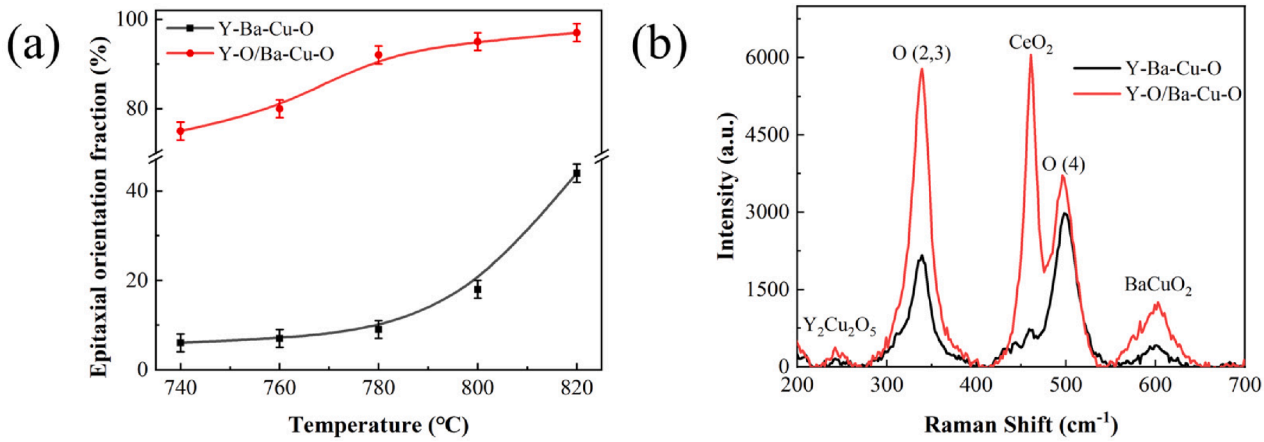

Fig. 6. Y-Ba-Cu-O single-layer (black) and Y-O/Ba-Cu-O stacked-layer (red) films after sintering: (a) f_X calculated from XRD results, (b) Raman spectra results. (For interpretation of the references to color in this figure legend, the reader is referred to the web version of this article.)

distribution of *a*- and *c*-axis orientations. XRD with a two-dimensional detector allows the simultaneous observation of *a*- and *c*-axis orientations and other texture components of YBCO.

We first investigated the orientation at different sintering temperatures for both Y-Ba-Cu-O single-layer and Y-O/Ba-Cu-O stacked-layer films. As shown in Fig. 6a, the f_X values in both types of films gradually increase with temperature. Thereby, the Y-Ba-Cu-O single-layer ranges at a significantly lower level, but shows a steeper rise towards higher temperatures and reaches f_X values of just over 40 % at 820 °C. The curve of the Y-O/Ba-Cu-O stacked-layer flattens out at higher temperatures and approaches f_X values of 100 % at 820 °C. Above all, however, it is over 75 % in the entire temperature range studied and therefore considerably higher than in the Y-Ba-Cu-O single-layer films.

Fig. 6b shows the Raman spectra of the Y-Ba-Cu-O single-layer and Y-O/Ba-Cu-O stacked-layer films. Two distinct peaks at the Raman shift of ~336 cm ^{1} and ~500 cm ^{1} correspond to the vibrational modes of oxygen at the CuO_2 planes (O (2,3) out-of-phase) and into apical sites (O4) of orthorhombic $YBa_2Cu_3O_{7\ y}$, respectively. The wavenumber and the intensity ratio are consistent with a sharp *c*-axis crystal orientation [46–48]. The *c*-axis oriented grain fraction can be calculated from the following equation [49]:

$$I_R = f_R I_c + (1 \quad f_R) I_a \tag{4}$$

$$r = \frac{I_{B1g}}{I_{Ag}} = \frac{f_R I_{c_{B_{1g}}} + (1 \quad f_R) I_{a_{B_{1g}}}}{f_R I_{c_{A_g}} + (1 \quad f_R) I_{a_{A_g}}} \tag{5}$$

where I_{B1g} and I_{Ag} are the Raman intensity of the O (2,3)-B_{1g} and O (4)-A_g modes, respectively.

According to the Raman tensor elements reported in the literature [50], f_R can also be expressed by the following equation from a simple transformation of equation (5):

$$r = \frac{f_R\left(x^2_{B_{1g}} + y^2_{B_{1g}}\right) + (1 \quad f_R)(x^2_{B_{1g}} + z^2_{B_{1g}})}{f_R\left(x^2_{A_g} + y^2_{A_g}\right) + (1 \quad f_R)(x^2_{A_g} + z^2_{A_g})} \tag{6}$$

where the Raman tensor elements $x^2_{A_g} = y^2_{A_g} = 2$, $x^2_{B_{1g}} = y^2_{B_{1g}} = 8.5$, $z^2_{A_g} = 100$, and $z^2_{B_{1g}} \approx 0$. Therefore, equation (6) can be simplified and rearranged to:

$$f_R = \frac{r\left(z^2_{A_g} + x^2_{A_g}\right) \quad x^2_{B_{1g}}}{r\left(z^2_{A_g} \quad x^2_{A_g}\right) + x^2_{B_{1g}}} = \frac{102 \bullet r \quad 8.5}{98 \bullet r + 8.5} \tag{7}$$

Calculations based on the Raman spectra, Fig. 6b, give f_R values of $f_{R-single} = 0.82$ and $f_{R-stacked} = 0.93$ for the Y-Ba-Cu-O single-layer and the

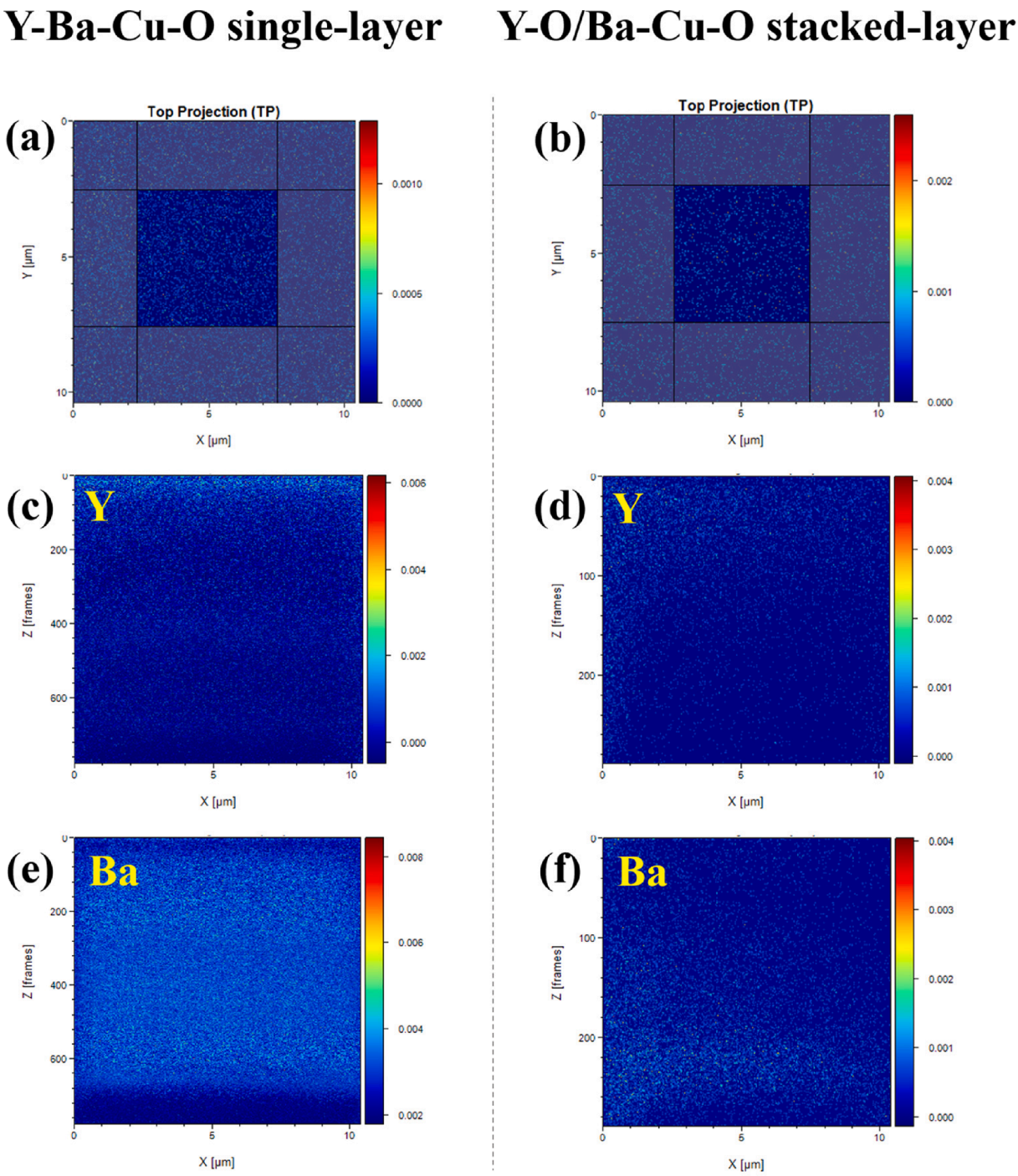

Fig. 7. TOF-SIMS 2D elemental images representing the distribution of Y and Ba signals. Top views of (a) Y-Ba-Cu-O single-layer film and (b) Y-O/Ba-Cu-O stacked-layer film, side views of (c) and (e) Y-Ba-Cu-O single-layer film, side views of (d) and (f) Y-O/Ba-Cu-O stacked-layer film. The region of interest is restricted to the black rectangular box.

Y-O/Ba-Cu-O stacked-layer film, respectively. From both the XRD and Raman spectra results, it is concluded that the Y-O/Ba-Cu-O stacked-layer structure of the precursor film can effectively increase D of yttrium in the Ba-Cu-O liquid phase, therefore suppressing random orientations, which is beneficial for the growth of c-axis orientated YBCO.

3.3. *Elemental diffusion behaviors and crystallization*

In order to understand the elemental distribution along the film thickness direction during the reaction–diffusion process, we analyzed films sintered from a Y-Ba-Cu-O single-layer and a Y-O/Ba-Cu-O stacked-layer by TOF-SIMS, as shown in Figs. 7 and 8. Both films were obtained by quenching at 780 °C. It can be clearly seen that yttrium is enriched on the surface layer, while barium is rather uniformly distributed, which agrees with our previous results of YBCO studied by TEM and SIMS. In the Y-O/Ba-Cu-O stacked-layer film, the concentration of yttrium (Fig. 7d and Fig. 8b) decreases gradually from the film surface to the reaction site at the interface, indicating that the Ba-Cu-O precursor indeed increases D and thus reduces δ of the reaction. Besides, barium is mainly concentrated near the interface (Fig. 7f and Fig. 8b), which is consistent with our precursor structure. Therefore, TOF-SIMS results

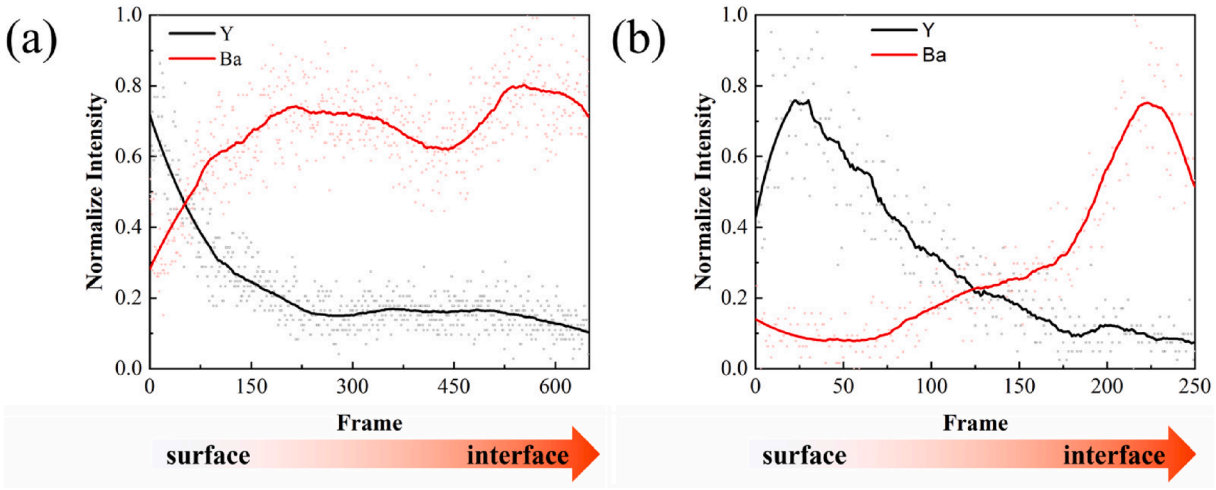

Fig. 8. TOF-SIMS depth profiles of (a) the Y-Ba-Cu-O single-layer film, (b) the Y-O/Ba-Cu-O stacked-layer film. The arrows represent the direction from the film surface to the interface. The data were acquired from the region of interest marked in Fig. 7 (central 5 × 5 μm^2).

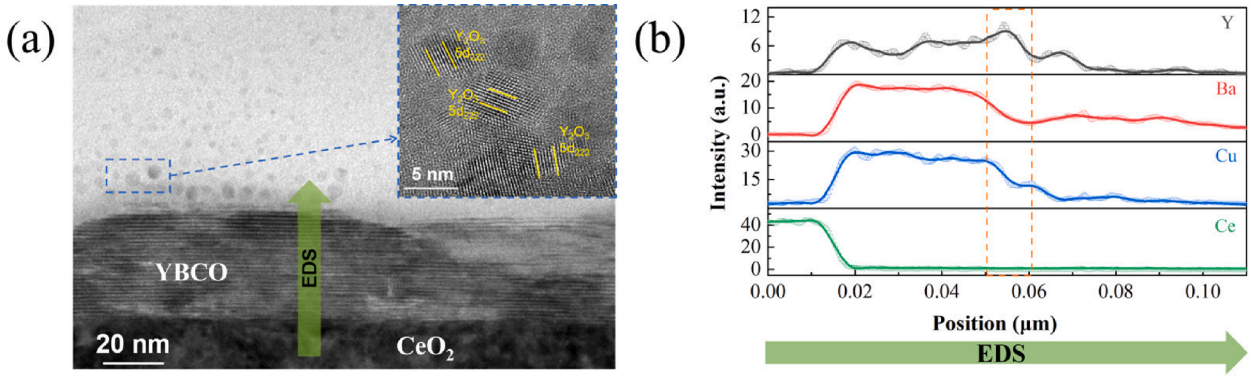

Fig. 9. (a) TEM image of a film sintered from a Y-O/Ba-Cu-O stacked-layer, (b) EDS line scans along the thickness direction for Y, Ba, Cu, and Ce, where dashed-line boxes represent the growth front.

again confirm the increase of *D* in Y-O/Ba-Cu-O stacked-layer films.

To further understand the interfacial nucleation behavior of the Y-O/Ba-Cu-O stacked-layer film, TEM and EDS analyses were carried out, Fig. 9. A small and well crystallized YBCO grain is visible at the interface, which has an epitaxial relationship to the CeO_2 buffer layer underneath. A few tens of nanometers above the YBCO crystal nucleus, a large number of spherical particles are detected, which tend to increase in size, the closer they appear to the YBCO growth front. These particles have average diameters of ~5 nm and can be identified as Y_2O_3, Fig. 9a inset. The EDS results along the film thickness direction, Fig. 9b, show that a Y-rich region is present just above the YBCO growth front. These results suggest that Y_2O_3 particles dissolve in the Ba-Cu-O liquid phase and preferentially form YBCO nuclei at the interface, which is consistent with our previous results.

4. Conclusion

We systematically studied the effect of supersaturation on the orientation in FF-MOD derived *RE*BCO films. According to the RE_2O_3-Ba-Cu-O phase diagram, different rare earth elements, sintering temperatures as well as concentrations of RE_2O_3 were adjusted to modulate supersaturation. The results reveal that low supersaturation is favorable to grow *c*-axis oriented *RE*BCO films by the FF-MOD method. Moreover, a stacked-layer architecture of Y-O/Ba-Cu-O was designed to modulate the diffusion distance to the reaction site *D* of yttrium through the Ba-Cu-O liquid phase to the reaction site at the interface. Cross-sectional TEM analysis shows that the diffusion of yttrium indeed could pass through the Y-O/Ba-Cu-O stacked-layer. Combined XRD and Raman spectroscopy analyses suggest that large *D* values of yttrium allow to significantly reduce supersaturation, therefore, enhancing the *c*-axis orientation growth. This work sheds light on the reaction mechanism of YBCO derived from the FF-MOD route, and demonstrates the influence of supersaturation control on the growth of films with preferential orientations.

Declaration of Competing Interest

The authors declare that they have no known competing financial interests or personal relationships that could have appeared to influence the work reported in this paper.

Data availability

No data was used for the research described in the article.

Acknowledgments

The authors would like to acknowledge financial support from the National Key R&D Program of China (No. 2022YFE03150201), the National Natural Science Foundation of China (Grant No. 52277027), the Scientific Research Program of Science and Technology commission of Shanghai Municipality (Grant No. 21XD1430700), and the Shanghai

Pujiang Program (21PJD097). We thank the Instrument Analysis Center of Shanghai Jiao Tong University for Raman spectroscopy and TOF-SIMS measurements. The authors also acknowledge the China Scholarship Council (CSC).

References

[1] R.W. Schwartz, Chemical solution deposition of perovskite thin films, Chem. Mater. 9 (11) (1997) 2325–2340.

[2] R.W. Schwartz, T. Schneller, R. Waser, Chemical solution deposition of electronic oxide films, Comptes Rendus Chimie 7 (5) (2004) 433–461.

[3] Q. Zhang, D. Sando, V. Nagarajan, Chemical route derived bismuth ferrite thin films and nanomaterials, J. Mater. Chem. C 4 (19) (2016) 4092–4124.

[4] B.D. Ahn, H.J. Jeon, J.S. Park, Effects of Ga: N addition on the electrical performance of zinc tin oxide thin film transistor by solution-processing, ACS Appl. Mater. Interfaces 6 (12) (2014) 9228–9235.

[5] H. Takiyama, Supersaturation operation for quality control of crystalline particles in solution crystallization, Adv. Powder Technol. 23 (3) (2012) 273–278.

[6] G. Coquerel, Crystallization of molecular systems from solution: phase diagrams, supersaturation and other basic concepts, Chem. Soc. Rev. 43 (7) (2014) 2286–2300.

[7] M. Barrett, M. McNamara, H. Hao, P. Barrett, B. Glennon, Supersaturation tracking for the development, optimization and control of crystallization processes, Chem. Eng. Res. Des. 88 (8) (2010) 1108–1119.

[8] C. Guo, Z. Zhang, Y. Wu, Y. Wang, G. Ma, J. Shi, Z. Zhong, Z. Hong, Z. Jin, Y. Zhao, Synergic realization of electrical insulation and mechanical strength in liquid nitrogen for high-temperature superconducting tapes with ultra-thin acrylic resin coating, Supercond. Sci. Technol. 35 (7) (2022).

[9] C. Barth, G. Mondonico, C. Senatore, Electro-mechanical properties of REBCO coated conductors from various industrial manufacturers at 77 K, self-field and 4.2 K, 19 T, Supercond. Sci. Technol. 28 (4) (2015).

[10] Y. Wu, Y. Zhao, X. Han, G. Jiang, J. Shi, P. Liu, M.Z. Khan, H. Huhtinen, J. Zhu, Z. Jin, Y. Yamada, Ultra-fast growth of cuprate superconducting films: dual-phase liquid assisted epitaxy and strong flux pinning, Mater. Today Phys. 18 (2021).

[11] K. Tsuchiya, A. Kikuchi, A. Terashima, K. Norimoto, M. Uchida, M. Tawada, M. Masuzawa, N. Ohuchi, X. Wang, T. Takao, S. Fujita, Critical current measurement of commercial REBCO conductors at 4.2 K, Cryogenics 85 (2017) 1–7.

[12] S. Hahn, K. Kim, K. Kim, X. Hu, T. Painter, I. Dixon, S. Kim, K.R. Bhattarai, S. Noguchi, J. Jaroszynski, D.C. Larbalestier, 45.5-tesla direct-current magnetic field generated with a high-temperature superconducting magnet, Nature 570 (7762) (2019) 496–499.

[13] X.H. Zong, Y.W. Han, C.Q. Huang, Introduction of 35-kV kilometer-scale high-temperature superconducting cable demonstration project in Shanghai, Superconductivity 2 (2022).

[14] S. Yokoyama, J. Lee, T. Imura, T. Matsuda, R. Eguchi, T. Inoue, T. Nagahiro, H. Tanabe, S. Sato, A. Daikoku, T. Nakamura, Y. Shirai, D. Miyagi, M. Tsuda, Research and development of the high stable magnetic field ReBCO coil system fundamental technology for MRI, IEEE Trans. Appl. Supercond. 27 (4) (2017) 1–4.

[15] A. Razek, T. Benkel, Y. Miyoshi, X. Chaud, A. Badel, P. Tixador, REBCO tape performance under high magnetic field, Eur. Phys. J. Appl. Phys. 79 (3) (2017).

[16] X. Wang, W. Wang, Y. Lei, Y. Gao, S. Huang, X. Liu, Q. Zhou, Electromagnetic design of 1.5 T no-insulation REBCO coil system charged by multiflux pumps for dedicated MRI, IEEE Trans. Appl. Supercond. 29 (5) (2019) 4601805.

[17] X. Wang, D.R. Dietderich, J. DiMarco, W.B. Ghiorso, S.A. Gourlay, H.C. Higley, A. Lin, S.O. Prestemon, D.V.D. Laan, J.D. Weiss, A 1.2 T canted cosθ dipole magnet using high-temperature superconducting CORC® wires, Supercond. Sci. Technol. 32 (7) (2019), 075002.

[18] J.L. MacManus-Driscoll, S.C. Wimbush, Processing and application of high-temperature superconducting coated conductors, Nat. Rev. Mater. 6 (7) (2021) 587–604.

[19] P. Cayado, M. Erbe, S. Kauffmann-Weiss, C. Bühler, A. Jung, J. Hänisch, B. Holzapfel, Large critical current densities and pinning forces in CSD-grown superconducting $GdBa_2Cu_3O_{7-x}$ -BaHfO3 nanocomposite films, Supercond. Sci. Technol. 30 (9) (2017).

[20] A. Queralto, J. Banchewski, A. Pacheco, K. Gupta, L. Saltarelli, D. Garcia, N. Alcalde, C. Mocuta, S. Ricart, F. Pino, X. Obradors, T. Puig, Combinatorial screening of cuprate superconductors by drop-on-demand inkjet printing, ACS Appl. Mater Interfaces 13 (7) (2021) 9101–9112.

[21] C. Pop, B. Villarejo, F. Pino, B. Mundet, S. Ricart, M. de Palau, T. Puig, X. Obradors, Growth of all-chemical high critical current $YBa_2Cu_3O_{7-\delta}$ thick films and coated conductors, Supercond. Sci. Technol. 32 (1) (2019).

[22] X. Obradors, T. Puig, Z. Li, C. Pop, B. Mundet, N. Chamorro, F. Vallés, M. Coll, S. Ricart, B. Vallejo, F. Pino, A. Palau, J. Gázquez, J. Ros, A. Usoskin, Epitaxial $YBa_2Cu_3O_{7-x}$ nanocomposite films and coated conductors from BaMO3 (M = Zr, Hf) colloidal solutions, Supercond. Sci. Technol. 31 (4) (2018).

[23] X. Obradors, T. Puig, S. Ricart, M. Coll, J. Gazquez, A. Palau, X. Granados, Growth, nanostructure and vortex pinning in superconducting $YBa_2Cu_3O_7$ thin films based on trifluoroacetate solutions, Supercond. Sci. Technol. 25 (12) (2012), 123001.

[24] X. Obradors, F. Martínez-Julián, K. Zalamova, V.R. Vlad, A. Pomar, A. Palau, A. Llordés, H. Chen, M. Coll, S. Ricart, N. Mestres, X. Granados, T. Puig, M. Rikel, Nucleation and mesostrain influence on percolating critical currents of solution derived $YBa_2Cu_3O_7$ superconducting thin films, Phys. C: Supercond. Appl. 482 (2012) 58–67.

[25] H. Chen, K. Zalamova, A. Pomar, X. Granados, T. Puig, X. Obradors, Growth rate control and solid–gas modeling of TFA-$YBa_2Cu_3O_7$ thin film processing, Supercond. Sci. Technol. 23 (3) (2010).

[26] F.M. Granozio, M. Salluzzo, U.S.d. Uccio, Competition between a-axis and c-axis growth in superconducting thin films, Phys. Rev. B 61(1) (2000) 756–765.

[27] V.F. Solovyov, H.J. Wiesmann, M. Suenaga, Nucleation of $YBa_2Cu_3O_{7-x}$ on buffered metallic substrates in thick precursor films made by the BaF2 process, Supercond. Sci. Technol. 18 (3) (2005) 239–248.

[28] J.L. MacManus-Driscoll, J.C. Bravman, R.B. Beyers, Phase equilibria in the Y-B-Cu-O system and melt processing of Ag clad $Y_1Ba_2Cu_3O_{7-x}$ tapes at reduced oxygen partial pressures, Phys. C: Supercond. 241 (3–4) (1995) 401–413.

[29] L.S. Guo, Y.Y. Chen, X. Yao, Continuous change of supersaturation and evolution of oriented structure in dipping LPE process of $YBa_2Cu_3O_{7-\delta}$, J. Cryst. Growth 404 (2014) 69–74.

[30] Y. Wan, J. Qian, H. Xiang, S. Huang, W. Wang, X. Yao, A. Koblischka-Veneva, Evolution of oriented structures in $YBa_2Cu_3O_{7-\delta}$ films by liquid phase epitaxy through manipulating supersaturation, Cryst. Growth Des. 20 (5) (2020) 3334–3340.

[31] C.Y. Tang, Y.Y. Chen, W. Li, L.J. Sun, X. Yao, M. Jirsa, Supersaturation-controlled growth orientation and grain boundary transition in $REBa_2Cu_3O_{7-\delta}$ (RE = Sm, $Sm_{1-x}Y_x$) liquid-phase epitaxial films, Cryst. Growth Des. 10 (2) (2010) 575–579.

[32] V. Solovyov, I.K. Dimitrov, Q. Li, Growth of thick $YBa_2Cu_3O_7$ layers via a barium fluoride process, Supercond. Sci. Technol. 26 (1) (2013), 013001.

[33] H. Yamasaki, K. Ohki, I. Yamaguchi, M. Sohma, W. Kondo, H. Matsui, T. Manabe, T. Kumagai, Strong flux pinning due to dislocations associated with stacking faults in $YBa_2Cu_3O_{7-\delta}$ thin films prepared by fluorine-free metal organic deposition, Supercond. Sci. Technol. 23 (10) (2010), 105004.

[34] Y. Zhao, J. Chu, T. Qureishy, W. Wu, Z. Zhang, P. Mikheenko, T.H. Johansen, J.-C. Grivel, Structural and superconducting characteristics of $YBa_2Cu_3O_7$ films grown by fluorine-free metal-organic deposition route, Acta Mater. 144 (2018) 844–852.

[35] J. Chu, Y. Zhao, M.Z. Khan, X. Tang, W. Wu, J. Shi, Y. Wu, H. Huhtinen, H. Suo, Z. Jin, Insight into the interfacial nucleation and competitive growth of $YBa_2Cu_3O_{7-\delta}$ films as high-performance coated conductors by a fluorine-free metal-organic decomposition route, Cryst. Growth Des. 19 (11) (2019) 6752–6762.

[36] D.E. Wesolowski, Y.R. Patta, M.J. Cima, Conversion behavior comparison of TFA–MOD and non-fluorine solution-deposited YBCO films, Phys. C: Supercond. 469 (13) (2009) 766–773.

[37] L. Soler, J. Jareno, J. Banchewski, S. Rasi, N. Chamorro, R. Guzman, R. Yanez, C. Mocuta, S. Ricart, J. Farjas, P. Roura-Grabulosa, X. Obradors, T. Puig, Ultrafast transient liquid assisted growth of high current density superconducting films, Nat. Commun. 11 (1) (2020) 344.

[38] J. Shi, Y. Zhao, G. Jiang, J. Zhu, Y. Wu, Y. Gao, X. Quan, X. Yu, W. Wu, Z. Jin, Deposition of REBCO with different rare earth elements on CeO2 buffered technical substrates by fluorine-free metal organic decomposition route, J. Eur. Ceram. Soc. 41 (10) (2021) 5223–5229.

[39] Y. Zhao, P. Torres, X. Tang, P. Norby, J.C. Grivel, Growth of highly epitaxial $YBa_2Cu_3O_{7-\delta}$ films from a simple propionate-based solution, Inorg. Chem. 54 (21) (2015) 10232–10238.

[40] J. Chu, Y. Zhao, Y. Ji, W. Wu, J. Shi, Z. Hong, L. Ma, H. Suo, Z. Jin, Interface reaction-governed heteroepitaxial growth of $YBa_2Cu_3O_{7-\delta}$ film on CeO_2-buffered technical substrate, J. Am. Ceram. Soc. 102 (10) (2019) 5705–5715.

[41] Y. Zhao, J.M. Zhu, G.Y. Jiang, C.S. Chen, W. Wu, Z.W. Zhang, S.K. Chen, Y. M. Hong, Z.Y. Hong, Z.J. Jin, Y. Yamada, Progress in fabrication of second generation high temperature superconducting tape at Shanghai Superconductor Technology, Supercond. Sci. Technol. 32 (4) (2019), 044004.

[42] J. Shi, Y. Zhao, Y. Wu, J. Chu, X. Tang, X. Li, X. Yu, W. Wu, G. Jiang, H. Suo, Z. Jin, Pyrolysis behaviors dominated by the reaction–diffusion mechanism in the fluorine-free metal–organic decomposition process, J. Mater. Chem. C (2020) 1–12.

[43] M. Murakami, N. Sakai, T. Higuchi, S.I. Yoo, Melt-processed light rare earth element - Ba-Cu-O, Supercond. Sci. Technol. 9 (1996).

[44] J. Chu, Y. Zhao, G. Jiang, W. Wu, Z. Zhang, Z. Hong, Z. Jin, Surface engineering of the flexible metallic substrate by SDP-Gd-Zr-O layer for IBAD-MgO templates, J. Am. Ceram. Soc. (2018).

[45] T. Aselage, K. Keefer, Liquidus relations in Y-Ba–Cu oxides, J. Mater. Res. 3 (6) (1988) 1279–1291.

[46] C. Camerlingo, I. Delfino, M. Lepore, Micro-Raman spectroscopy on YBCO films during heat treatment, Supercond. Sci. Technol. 15 (11) (2002) 1606.

[47] M. Iliev, P. Zhang, H.-U. Habermeier, M. Cardona, Raman spectroscopy as analytical tool for the local structure of YBa2Cu3Ox thin films, J. Alloy. Compd. 251 (1–2) (1997) 99–102.

[48] E. García-González, G. Wagner, M. Reedyk, H.U. Habermeier, Microstructural analysis of YBa2Cu3Oythin films deposited on SrTiO3and LaAlO3substrates by off-axis magnetron sputtering, J. Appl. Phys. 78 (1) (1995) 353–359.

[49] J.C. González González, Coated conductors and chemical solution growth of YBCO films a micro-raman spectroscopy study, Universitat Autònoma de Barcelona, 2005.

[50] N. Dieckmann, R. Kiirsten, M. LOhndorf, A. Bock, Epitaxial quality of *c*-axis and *a*-axis oriented $YBa_2Cu_3O_7$ films Characterization by Raman spectroscopy, Phys. C: Supercond. Appl. 245 (3) (1995) 212–218.